GPS Solutions (2024) 28:172
https://doi.org/10.1007/s10291-024-01723-6

ORIGINAL ARTICLE

Real-time LEO satellite clock estimation with predicted LEO satellite orbits constrained

Wei Xie[1,2] · Hang Su[1,2] · Kan Wang[1,2,3] · Jiawei Liu[1,2] · Meifang Wu[1,2,3] · Min Zou[1,2,3] · Ahmed El-Mowafy[4] · Xuhai Yang[1,2,3]

Received: 6 May 2024 / Accepted: 30 July 2024

Abstract

Low Earth Orbit (LEO) satellites can augment the traditional GNSS-based positioning, navigation and timing services, which require real-time high-precision LEO satellite clock products. As the complicated systematic effects contained in the LEO satellite clock estimates limit their high-precision mid- to long-term prediction, high-frequency LEO satellite clocks need to be estimated within a Kalman filter, resulting in a short prediction time for real-time applications. Compared to the clock estimation using Batch Least-Squares (BLS) adjustment, filter-based clock estimation experiences a lower precision. Increasing the model strength by introducing external orbital information, thus, de-correlating the orbital and clock parameters, will benefit real-time clock precision. In this contribution, reduced-dynamic LEO satellite orbits are first estimated using BLS adjustment in near real-time and predicted in the short term. The predicted orbits are then constrained during the Kalman-filter-based clock estimation process. The variance–covariance matrix of the introduced orbital errors is tested for different sets of values in the radial, along-track and cross-track directions when constraining orbits of different prediction times. One week of GPS data from the Sentinel-3B satellite in 2018 was used for validation of the proposed method. When weakly constraining high-accuracy predicted orbits within a prediction time of 20 min, i.e., with a standard deviation of the constraint set to 2–3 dm in the radial and cross-track directions, and 4–6 dm in the along-track direction, the estimated clock accuracy can be improved from about 0.27 to 0.23 ns, with a 13.4% improvement. Depending on the prediction period of the introduced orbits, the Signal-In-Space Range Error (SISRE) of the LEO satellite to Earth can also be improved, from about 9.59 cm without constraints, to 7.38–8.07 cm after constraining the predicted orbits, with an improvement of 16–23%. The improvements in the SISRE also indicate a better consistency between the real-time clock and orbital estimates.

Keywords Real-time · Low Earth Orbit (LEO) · Clock estimation · Orbital constraints

Introduction

Low Earth Orbit (LEO) satellites were proposed to provide a rapid LEO-enhanced Global Navigation Satellite System (GNSS) real-time Precise Point Positioning (PPP) services (Ke et al. 2015; Li et al. 2019a, 2024) for ground users owing to LEO's rapid motion, resulting in a fast geometry variation (Li et al. 2019b). The real-time orbital and clock products of LEO satellites are two key prerequisites for conducting LEO-enhanced real-time PPP services.

While the real-time LEO satellite orbits can be predicted with an accuracy of a few centimeters within a prediction time of 15 min (Wang et al. 2023a), generating high-precision and real-time LEO satellite clock products is still a challenge. Compared to the GNSS satellite clocks, mid-term LEO satellite clock prediction exhibits a rather significant degradation in its precision with the increase in prediction time due to the systematic effects detected in various LEO satellite clock estimates (Wang and El-Mowafy 2022; Ge et al. 2023; Wu et al. 2023). For example, the satellite clocks of the Gravity Recovery and Climate Experiment

✉ Kan Wang
wangkan@ntsc.ac.cn

1 National Time Service Center, Chinese Academy of Sciences, Xi'an 710600, China

2 Key Laboratory of Time Reference and Applications, Chinese Academy of Sciences, Xi'an 710600, China

3 University of Chinese Academy of Sciences, Beijing 100049, China

4 School of Earth and Planetary Sciences, Curtin University, Perth, WA 6845, Australia

Published online: 06 August 2024

(GRACE)-FO 1 and Sentinel-3B showed meter-level periodic behaviors that were supposed to be related to the temperature and/or the South Atlantic Anomaly (SAA), not to mention the complicated relativistic effects contained in the LEO satellite clock estimates (Wang and El-Mowafy 2022). Attempts using trigonometrical functions (Wang and El-Mowafy 2022), least-square harmonic estimation (Ge et al. 2023), and removing the relativistic effects analytically (Wu et al. 2023) still leave a precision loss at sub-nanoseconds for clock predictions over 10 to 15 min, which is remarkably poorer than those of GNSS satellite clocks (Xie et al. 2021). As a result, Kalman-filter-based high-frequency clock estimation is considered a reasonable strategy for producing high-precision real-time LEO satellite clocks due to the short prediction time (such as within 30 min) applied.

The strategies for Kalman-filter-based LEO satellite clock estimation can be divided into two cases, i.e., using and not using a ground network that receives LEO satellite navigation signals. The former case makes use of a stronger observation model by employing the navigation signals from the LEO satellite to the ground network and directly estimates the LEO satellite hardware biases of the transmitter needed by ground users (Yang et al. 2020; 2022). However, the low altitudes of LEO satellites require eventually a very dense network distribution over the entire Earth for continuously acquiring LEO satellites signals (Wang et al. 2022b). When not using a ground network for LEO satellite clock determination, the LEO satellite clocks can be estimated as independent epoch parameters using the GNSS observations tracked onboard LEO satellites, combined or not combined with the dynamic models (Yunck et al. 1994; Li et al. 2017; Mao et al. 2021; Kunzi and Montenbruck 2022; El-Mowafy et al. 2023). With the clock precision is of less interest than the orbital accuracy, the filter-based estimated real-time clock precision is not discussed. A real-time clock precision of 0.9 ns was reported when using a real-time reduced-dynamic approach (Kunzi and Montenbruck 2022). In Yang et al. (2022), 0.15 and 0.39 ns were achieved when integrating and not integrating a ground network with the LEO onboard, respectively. A major reason for obtaining sub-optimal real-time LEO satellite clock precision is its correlation with the orbital parameters.

Because the GNSS satellite orbits can be predicted with enough high precision in the short to mid-term (such as 1–6 h) (Duan et al. 2019), the predicted GNSS satellite orbits are often introduced when estimating GNSS real-time satellite clocks (Fu et al. 2023). Similarly, the short-term predicted LEO satellite orbit can also be applied to LEO satellite clock estimation as high accuracy of a few centimeters can be achieved within a short-term orbital prediction (Wang et al. 2023b). This contribution focuses on improving the real-time LEO satellite clock precision by introducing and properly constraining the short-term prediction of LEO satellite orbits, i.e., the estimated LEO satellite orbits are set equal to the independently predicted orbits computed based on the BLS POD methodology with a pre-defined variance–covariance matrix. This, on the one hand, de-correlates the orbit and the clock parameters, and thus improves model strength. On the other hand, this improves the consistency between the real-time orbital and clock products provided to users, i.e., delivering a better combined orbital and clock precision. In this contribution, real data from the LEO satellite Sentinel-3B is used for validation of the proposed method. Different constraints are applied and tested for LEO satellite orbits at different prediction intervals, i.e., with different accuracies. Its impacts on the real-time clock precision and the Signal-In-Space Ranging Error (SISRE) from the LEO satellite to the Earth are comprehensively analyzed.

The paper starts with a description of the methods, including those for the near-real-time LEO satellite Precise Orbit Determination (POD) and orbit prediction, real-time LEO satellite clock estimation, and constraining of predicted LEO satellite orbits. Next, the experimental setup is discussed, and the results are analyzed in terms of the performance of the predicted orbits, the estimated clocks, orbits and SISRE. The conclusions are given at the end.

Methods

In this section, the strategy for near-real-time LEO satellite POD and its prediction is first briefly discussed. The model for real-time LEO satellite clock estimation is then described in detail, with the constraining method of the predicted orbits explained next. The data processing chart is given at the end of the section.

Near-real-time LEO satellite POD and prediction

The LEO satellite orbits can be determined in the reduced-dynamic mode (Yunck et al. 1994) using dynamic models and dual-frequency GNSS code and phase observations tracked onboard the LEO satellite. The Ionospheric-Free (IF) combined observation equations can be used to improve the estimable dynamic parameters, which can be expressed as at the epoch i:

$$E\left(P^s_{r,IF}(t_i)\right) = A^s_D(t_i)\bullet X_K + A^s_{SRP}(t_i)\bullet p_{SRP} + A^s_{Sto}(t_i)\bullet a_{Sto} + c\times t_{r,IF}(t_i) \quad (1)$$

$$E\left(L^s_{r,IF}(t_i)\right) = A^s_D(t_i)\bullet X_K + A^s_{SRP}(t_i)\bullet p_{SRP} + A^s_{Sto}(t_i)\bullet a_{Sto} + c\times t_{r,IF}(t_i) + \lambda_{IF}\times N^s_{r,IF}(t_i) \quad (2)$$

where $E(\bullet)$ is the expectation operator. s and r represent the GNSS and LEO satellites, respectively. $P^s_{r,IF}$ and $L^s_{r,IF}$ are code and phase Observed-Minute-Computed (OMC) terms, respectively. OMC refers to the IF code and phase observations minus the computed ranges. The latter is computed based on the estimated LEO position (initially best approximate values, updated with solution iteration), the LEO and GNSS satellite orbits, the GNSS satellite clocks, the GNSS and LEO satellite Phase Center Offsets (PCOs) and Variations (PCVs), and the relativistic effects, etc. A^s_D, A^s_{SRP} and A^s_{Sto} represent the partial derivatives of the IF observations with respective to X_K, p_{SRP} and a_{Sto}, respectively. X_K denotes the vector containing six Keplerian elements for the LEO satellite at the initial epoch t_0. p_{SRP} and a_{Sto} are Solar Radiation Pressure (SRP) parameters and piece-wise constant stochastic accelerations set every few minutes to compensate for efficiencies in existing models, respectively. c is the speed of light, and $t_{r,IF}$ is the estimable LEO satellite clock, containing the LEO satellite IF code bias (Kouba 2009) and the LEO satellite relativistic effects. λ_{IF} is the IF wavelength, and $N^s_{r,IF}$ is a mathematical expression arising from the IF combined ambiguities. The PCOs and PCVs, relativistic effects of the GNSS satellites, and phase wind-up effects are corrected in the OMC terms. With the dynamic parameters, i.e., X_K, p_{SRP} and a_{Sto} estimated using high-precision real-time GNSS orbital and clock products applying a Batch Least-Squares (BLS) adjustment (Wang et al. 2023b), in which the observations from multi-epoch are simultaneously processing using the least-squares adjustment, then the LEO satellite orbits at each epoch can be obtained by numerical integration (Beutler 2005).

The near-real-time POD results are next predicted in the short term within tens of minutes. Based on previous studies for LEO satellite prediction (Wang et al. 2022a, 2023b), the six Keplerian elements, the constant (a_{R0}, a_{A0}, a_{C0}), sine (a_{RS}, a_{AS}, a_{CS}), and cosine terms (a_{RC}, a_{AC}, a_{CC}) of the 3-dimensional (3D) SRPs are estimated with a least-squares adjustment using the last four hours of the POD results. The SRP-induced accelerations in the radial ($a_{SPR,R}$), along-track ($a_{SPR,A}$) and cross-track ($a_{SPR,C}$) directions can be expressed as:

$$a_{SPR,R} = a_{R0} + a_{RC} \times cos(U) + a_{RS} \times sin(U) \tag{3}$$

$$a_{SPR,A} = a_{A0} + a_{AC} \times cos(U) + a_{AS} \times sin(U) \tag{4}$$

$$a_{SPR,C} = a_{C0} + a_{CC} \times cos(U) + a_{CS} \times sin(U) \tag{5}$$

where U is the argument of latitude. With the fitted orbital dynamic parameters, the predicted LEO satellite orbits can be numerically integrated into the epoch within a short period (Beutler 2005).

Real-time LEO satellite clock estimation

The dual-frequency GNSS IF combined code and carrier phase observations are used to estimate the LEO satellite clocks in real-time. For a GNSS-LEO satellite pair, they can be expressed as:

$$P^s_{r,IF} = \left(\mu^s_r\right)^{\mathrm{T}} \bullet \Delta x + c \times t_{r,IF} + \varepsilon^s_{r,IF} \tag{6}$$

$$L^s_{r,IF} = \left(\mu^s_r\right)^{\mathrm{T}} \bullet \Delta x + c \times t_{r,IF} + \lambda_{IF} \times N^s_{r,IF} + e^s_{r,IF} \tag{7}$$

where the symbol $P^s_{r,IF}$ and $L^s_{r,IF}$, c, $t_{r,IF}$, λ_{IF} and $N^s_{r,IF}$ have the same explanations as in Eqs. (1) and (2). μ^s_r is the unit vector from GNSS s to LEO satellite r, and Δx is the vector of the LEO satellite orbital increments relative to the a priori orbits. $\varepsilon^s_{r,IF}$ and $e^s_{r,IF}$ are the combined measurement noise and multipath effects for code and carrier phase observations, respectively. The short-term predicted orbits are constrained as pseudo-observations with pre-defined uncertainties tested with different values. Then the error equation can be expressed as:

$$V_k = H_k \hat{x} - L_k \tag{8}$$

where V_k is the posterior residual matrix for all code and carrier phase observations, H_k is the design matrix for LEO satellite orbit, clock offset, and ambiguities (Kouba 2009), $\hat{x}$ is the estimated parameters, i.e., LEO satellite orbit, clock offset, and ambiguities. L_k is OMC for each code and carrier phase observation. The constrained equations and the corresponding dispersions are:

$$E\left(\hat{x}_{pre}\right) = \mathrm{x},\ \mathrm{D}\left(\hat{x}_{pre}\right) = D_{rac} \tag{9}$$

where $E\left(\hat{x}_{pre}\right)$ denotes the expectation of the predicted orbits $\hat{x}_{pre}$ introduced into the processing. Its dispersion $D\left(\hat{x}_{pre}\right)$ is represented by D_{rac}, which will be further discussed in the next subsection.

The Kalman filter (Kalman 1960) is applied to estimate the unknown parameters, with the data processing performed with the following equations:

$$\hat{X}_{k,k-1} = \Phi_{k,k-1} \hat{X}_{k-1} \tag{10}$$

$$P_{k,k-1} = \Phi_{k,k-1} P_{k-1} \Phi^T_{k,k-1} + S \tag{11}$$

$$K_k = P_{k,k-1} H^T_k \left(H_k P_{k,k-1} H^T_k + R_k\right)^{-1} \tag{12}$$

$$\hat{X}_k = \hat{X}_{k,k-1} + K_k \left(L_k - H_k \hat{X}_{k,k-1}\right) \tag{13}$$

$$P_k = (I - K_k H_k) P_{k,k-1} \tag{14}$$

The first two equations refer to the filter time update, whereas the last three equations describe the filter observations update. where $\widehat{X}_{k,k-1}$ and $P_{k,k-1}$ are one-step predicted values and their variance–covariance matrix for LEO satellite orbit, clock offset, and ambiguities, respectively. $\widehat{X}_{k-1}$ and P_{k-1} are estimated parameters from the previous epoch $k-1$ and its variance–covariance matrix for LEO satellite orbit, clock offset, and ambiguities, respectively. In practice, only the ambiguities are linked in time as constants, while the clocks and orbits are not linked in time. As such, $\widehat{X}_{k-1}$ contains ambiguities from the previous epoch and initial values for the orbits and clocks of the current epoch obtained from the Standard Point Positioning (SPP), in which the LEO satellite orbit and clock offset are epoch-wisely estimated using only GNSS broadcast ephemeris and code observations (Zhou and Wang 2023). $\Phi_{k,k-1}$ is the transition matrix, and the variance–covariance matrix for system noise has elements of zeros for ambiguities and very large values for orbits and clocks. S is the variance matrix for LEO satellite orbits. K_k is the gain matrix, and R_k is the variance matrix of observation noise. $\widehat{X}_k$ and P_k are the filtered estimates and their variance–covariance matrix, respectively.

Constraining the predicted orbits

In the traditional LEO satellite clock estimation, the LEO satellite orbits are weakly constrained to the SPP results based solely on code observations (Zhou and Wang 2023), with a variance of 60^2 m^2 (Kunzi and Montenbruck 2022). In this contribution, the estimable orbital elements are proposed to be constrained to the high-accuracy predicted LEO satellite orbits (see the last sub-section), obtained by using BLS near-real-time POD and short-term prediction (Wang et al. 2023b). Different variances of the constraints are tested. The model strength in this way is improved by de-correlating the orbits and clocks.

The LEO satellite orbital accuracy, especially that of the predicted orbits, differs in the along-track, cross-track, and radial directions. The along-track predicted LEO satellite orbits often suffer from poorer accuracy than those in the other two directions due to the air drag effects. As such, the variances for the orbital constraints are assumed different in the radial, along-track, and cross-track directions of the orbital system, with the root mean squares denoted as σ_{dR}, σ_{dA}, σ_{dC}, respectively. The variance matrix D_{rac} is expressed as:

$$D_{rac} = \begin{bmatrix} \sigma_{dR}^2 & 0 & 0 \\ 0 & \sigma_{dA}^2 & 0 \\ 0 & 0 & \sigma_{dC}^2 \end{bmatrix} \tag{15}$$

In this study, the cross-correlations among the orbital constraints in these directions are not considered, but could be an interesting topic to be addressed in future work.

As the orbital increments in Eqs. (6) and (7) are typically estimated and constrained in the Earth-Centered-Earth-Fixed (ECEF) system, D_{rac} is transformed to the ECEF system by propagation, expressed as:

$$D_{xyz} = M \bullet D_{rac} \bullet M^T \tag{16}$$

where M is the transformation matrix from the orbital system to the ECEF system, and D_{xyz} represents the transformed variance–covariance matrix of the orbital constraints in the ECEF system.

Data processing flowchart

The data processing flowchart of the proposed strategy for real-time LEO satellite clock determination by constraining predicted orbits is shown in Fig. 1. It can be divided into two parts, i.e., i) Data and products employed; ii) Data processing. The system first obtains the GNSS real-time satellite products, the LEO onboard GNSS observations, and all the needed model information. Errors like the GNSS satellite relativistic effects, the PCOs and PCVs of LEO and GNSS satellites, and the phase wind-up effects are corrected based on existing models (Kouba 2009), and initial LEO satellite clocks are estimated with the SPP. Thereafter, short-term predicted LEO satellite orbits estimated from BLS are introduced and constrained to update the OMC terms. The Kalman filter with proper constraints of the orbits is then employed to estimate all the unknown parameters, including LEO satellite orbits and clocks.

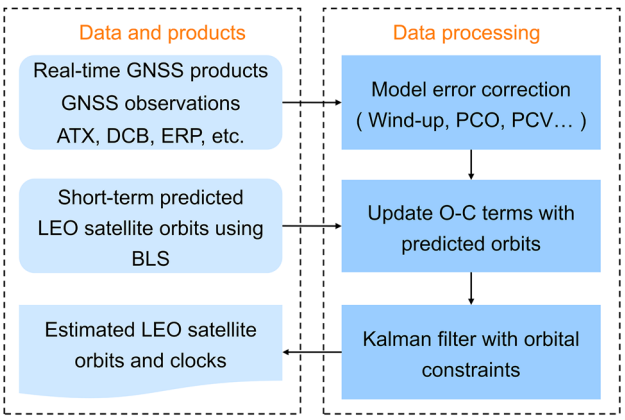

Fig. 1 Data processing flowchart for real-time LEO satellite clocks estimation constraining the predicted LEO satellite orbits

Experimental setup

To validate the proposed method, GPS data tracked by the LEO satellite Sentinel-3B was used in our experiment. This satellite was launched on 25 April 2018, and has an orbital altitude of 814.5 km, an eccentricity of 0.0001, an inclination of 98.65°, and an orbital period of about 1.7 h (Li et al. 2022; Wu et al. 2023).

The time scheme of LEO satellite POD and prediction strategy is shown in Fig. 2. The start time of the LEO satellite POD and prediction procedure is shifted by 5 min in each processing session, and the POD and prediction arc amount to 24 h and 30 min, respectively. For the predicted orbits, the first 20 min are separated into 4 parts, i.e., 0–5 min, 5–10 min, 10–15 min, and 15–20 min. Each part is termed the prediction time window.

The near-real-time LEO satellite POD and prediction strategies are shown in Table 1. GPS observations on L1/L2 frequency with a sample interval of 30 s from the Day Of Year (DOY) 226 to 232, 2018, were processed using the real-time GNSS satellite orbital and clock products of the Centre National d'Etudes Spatiales (CNES) (Laurichesse et al. 2013) in France. The wind-up and relativistic effects are modeled (Kouba 2009). The LEO satellite orbits from DOY 227 to 232 were predicted for 30 min. The dynamic models used for the reduced-dynamic POD are listed in Table 1.

For the real-time LEO satellite clock estimation constraining the predicted orbits, dual-frequency GPS L1/L2 signals with a sampling interval of 10 s were used to form the IF combination. The elevation mask angle was set to 3°. Similar to the POD process, the real-time GPS satellite orbital and clock products from the CNES (Laurichesse et al. 2013) were used. Kalman filtering (Kalman 1960) was employed to estimate the unknown parameters. Orbits of different prediction times were introduced in the clock estimation process, with the variances tested using seven different strategies. Detailed processing information is presented in Table 2 and the processing scenarios are discussed in the next section.

Experimental results

In this section, the LEO satellite orbits to be introduced and constrained are first assessed for different prediction times. The performances of the estimated clocks and orbits are then analyzed separately and in combined form, i.e., in the form of the SISRE.

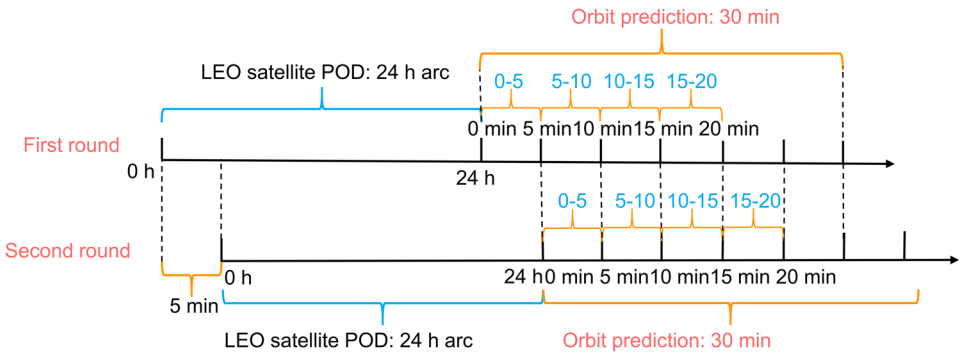

Fig. 2 Time scheme of LEO satellite POD and prediction strategy. The second round is shifted by 5 min from the first round, and this process is repeated for the following rounds

Table 1 Processing parameters for the near-real-time LEO satellite POD and prediction

Items	Strategies
POD arc	24 h
Sampling interval	30 s
Frequency	GPS L1/L2
GNSS satellite orbits/clocks	CNES real-time products
Estimator	BLS
Predicted arc	30 min
The gravitational attraction of the Earth	EGM2008 (degree: 120) (Pavlis et al. 2008)
Gravity of other planets	Planetary Ephemeris DE405 (Standish 1998)
Solid Earth tides	IERS 2010 (Petit and Luzum 2010)
Ocean tides	FES2004 (Lyard et al. 2006)

Table 2 Processing parameters for real-time LEO satellite clock estimation constraining the predicted orbits

Items	Parameters
Signals	GPS L1/L2
Observations	Dual-frequency IF combination
Elevation angle mask	3°
Sampling interval	10 s
GNSS real-time satellite orbits and clocks	CNES
Prediction time window of the introduced orbits	0–5, 5–10, 10–15, 15–20 min
Variances of the orbital constraints	Scenarios S1/S2/S3/S4/S5/S6/S7 (see Table 4)
Estimator	Kalman filter

Accuracy of the predicted LEO satellite orbits

As mentioned in the Section "Methods", the predicted LEO satellite orbits are introduced and constrained during the real-time clock estimation. The accuracy of the introduced orbits will surely impact the performance of the estimated clocks. In this sub-section, the performances of the predicted satellite orbits are assessed for different prediction times. Considering that the LEO satellite POD and prediction using the BLS method could be time-consuming depending on the processing unit used (Wang et al. 2023b), four prediction time windows are tested for the introduced orbits, i.e., 0–5, 5–10, 10–15, and 15–20 min. The post-processed final LEO satellite orbits obtained with a BLS adjustment using the final GNSS products of the Center for Orbit Determination in Europe (CODE) (Prange et al. 2017) were used as a reference.

As an example, Fig. 3 shows the orbital prediction errors of Sentinel-3B from 4:00 to 4:30 in GPS Time (GPST) on DOY 227 to 232, 2018. As the prediction time increases, the fluctuation of the along-track orbital errors (red lines) is larger than those in the cross-track and the radial directions within 30 min. This can be attributed to the air drag effect that influences mainly the along-track orbital prediction.

To assess the accuracy of the predicted orbits within different prediction windows, the entire process of the near-real-time POD and following orbit prediction is shifted by 5 min each time in the test period. The RMSE of the predicted LEO satellite orbits within different prediction time windows are shown in Fig. 4, with each point representing the RMSE of the orbits within the prediction time window of one prediction arc. As the predicted time in the tested time windows increases, the accuracy of the predicted LEO satellite orbits gradually degrades in all three directions, especially in the along-track directions (red dots), Since the prediction model cannot perfectly describe the real orbital situation, as the prediction time increases, the estimated dynamic parameters are becoming increasingly inaccurate, resulting in a worse accuracy of the predicted orbits. Furthermore, spikes around DOY 229 were caused by relatively low accuracies of the POD results during these periods.

Figure 5 illustrates the percentage values of the RMSE of the predicted orbits in the three directions for different prediction time windows. In the cross-track and radial directions (middle and right panels), the RMSE of the predicted orbits is less than 5 cm around or more than 90% of the time for all tested prediction time windows. In the along-track direction (left panel), the percentage

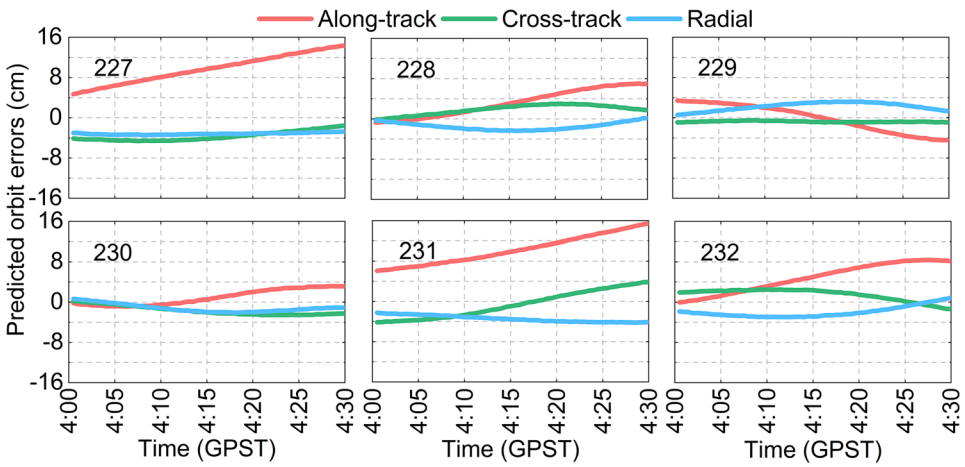

Fig. 3 LEO satellite orbital prediction errors within 30 min started at 4:00 (GPST) on DOY 227 to 232, 2018, for Sentinel-3B

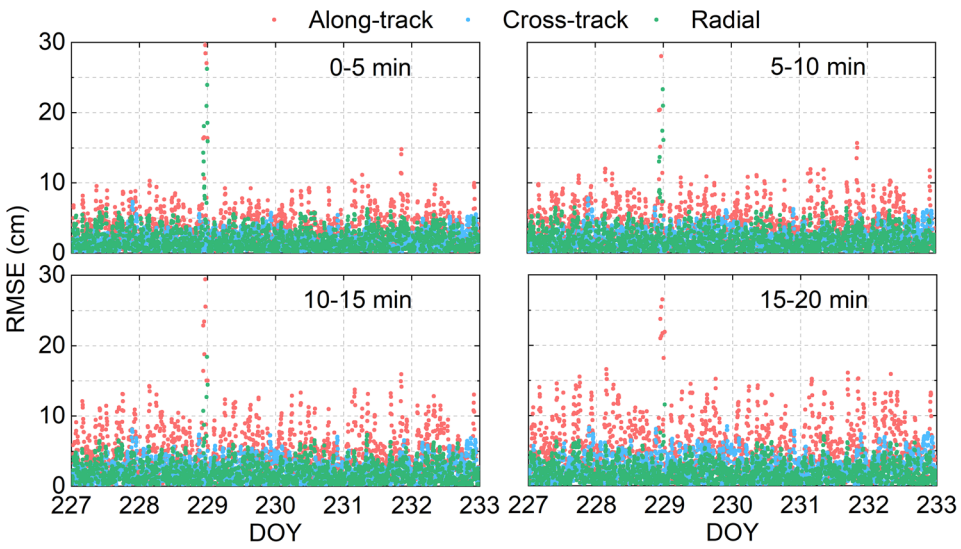

Fig. 4 Accuracy of the predicted LEO satellite orbits within different prediction time windows

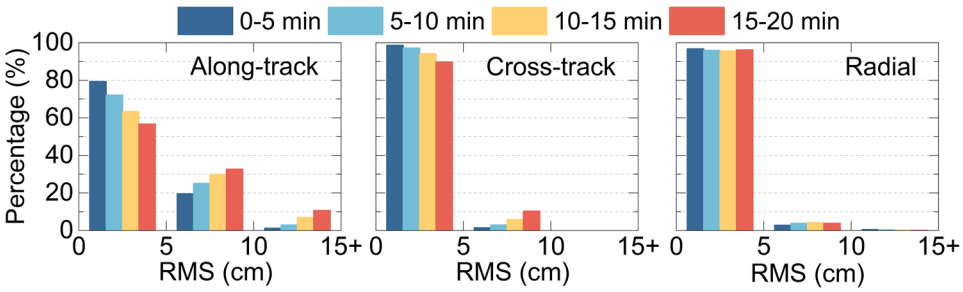

Fig. 5 Percentage values of the predicted orbital accuracy for different prediction time windows

Table 3 Average accuracy of the predicted orbits for Sentinel-3B over different prediction time windows

Direction	0–5 min (cm)	5–10 min (cm)	10–15 min (cm)	15–20 min (cm)
Along-track	4.57	5.31	6.00	6.63
Cross-track	2.14	2.42	2.75	3.08
Radial	2.75	2.68	2.56	2.45

Table 4 Variances of LEO satellite orbital constraints

Schemes	Along-track	Cross-track	Radial	Introduced orbits
S1	60^2 m^2	60^2 m^2	60^2 m^2	SPP
S2	4^2 cm^2	2^2 cm^2	2^2 cm^2	Predicted
S3	10^2 cm^2	5^2 cm^2	5^2 cm^2	Predicted
S4	20^2 cm^2	10^2 cm^2	10^2 cm^2	Predicted
S5	40^2 cm^2	20^2 cm^2	20^2 cm^2	Predicted
S6	60^2 cm^2	30^2 cm^2	30^2 cm^2	Predicted
S7	1^2 cm^2	1^2 cm^2	1^2 cm^2	Reference

of the predicted orbital accuracy within 0–5 cm amounts to 79.3%, 72.1%, 63.3%, and 56.7% for prediction time windows of 0–5, 5–10, 10–15 and 15–20 min, respectively.

Table 3 lists the average accuracy of the predicted orbits in the along-track, cross-track, and radial directions for different prediction time windows. As the prediction time grows, the accuracy of the predicted orbits decreases in the along-track and cross-track directions. When increasing the prediction time from 0–5 min to 15–20 min, the average RMSE increases from 4.57 to 6.63 cm in the along-track direction, and from 2.14 to 3.08 cm in the cross-track direction. This accuracy difference would influence the variances of the orbital constraints that will be used during clock estimation, and suggests the importance of an efficient and high-accuracy POD in this approach.

Performances of the real-time clock and orbital estimates

To validate the proposed method, seven schemes are designed for comparison and analysis (see Table 4). Scheme 1 (S1) represents the case of real-time LEO satellite clock estimation without introducing external orbits, where the estimated orbits are weakly constrained to the initial orbits obtained through the SPP with a very large

variance, i.e., 60^2 m^2 (Kunzi and Montenbruck 2022). When introducing predicted orbits of each prediction time window, S2 to S6 are tested with strong to weak orbital constraints. Considering the worse prediction accuracy in the along-track direction as shown in the last sub-section, the RMS in the along-track direction is set to be twice the size of those in the cross-track and radial directions. For comparison, the post-processed final LEO satellite orbits obtained with a BLS adjustment using the final GNSS products of the CODE (Prange et al. 2017) are also introduced and strongly constrained, i.e., with the variance set to 1^2 cm^2 in all three directions (S7). Detailed information on the orbital constraints for different schemes is shown in Table 4.

In real-time, the start time of the BLS POD arc (and orbit prediction afterward) is shifted by 5 min in each procession session. The orbits are predicted for 30 min, in which the first 20 min arc is divided into 4 prediction time window, i.e., 0–5 min, 5–10 min, 10–15 min and 15–20 min, where the length of each prediction time window is 5 min. The predicted orbits of the same prediction window (e.g., 0–5 min) over subsequent processing rounds (shifted by 5 min) are connected, so that they can be continuously introduced in the Kalman-filter-based clock estimation. The post-processed final LEO satellite clocks obtained with a BLS adjustment using the final GNSS products of the CODE (Prange et al. 2017) were used as a reference. The estimated real-time clocks were re-aligned to the final reference clocks before the assessment by computing the epoch-mean difference between the real-time GNSS clocks used and the final GNSS clocks (Huang et al. 2018).

The clock errors applying different schemes on DOY 230 are presented in Fig. 6. In S1 (red lines), the LEO satellite clocks were estimated without introducing external orbits. The patterns thus remain the same for all of the Figure subplots. Some spikes can be observed in S1, such as those near 8:00 in GPST. After employing strong constraints (i.e., with low uncertainty) like S2 and S3, the fluctuation of the clock estimates becomes larger, for example at 2:00 to 6:00, and 8:00 to 12:00, and this becomes more obvious for long prediction periods (see the bottom right panel). Although the RMS of the predicted orbital errors amounts only to a few centimeters (see Table 3), the introduced orbital errors are considered biases but not Gaussian noise as assumed in the variance–covariance matrix of the constraint equations. Due to the correlations between the orbits and clocks, the biases are pushed into clock estimates when constraining the introduced orbits too strongly. The fluctuation of the clock errors is significantly reduced when applying S4. When applying S5 and S6, the clock errors fluctuation become smaller compared to those of S4. The spikes that appeared in S1, and the fluctuations that appeared in S2 and S3 are reduced or disappeared, indicating a better performance of the clock estimation. In terms of S7, the clock errors exhibit the smallest fluctuation among these schemes. It can be concluded that improved clock performance can be achieved when constraining high-accuracy predicted LEO satellite orbits with appropriate constraints. The clock estimates constraining the predicted orbits at the prediction time window of 0–5 min show the best performance among the four cases, especially for the part between 12:00 and 16:00 (GPST).

For a better demonstration, the real-time clock precision achieved with different schemes is presented in Fig. 7. For each S scheme (i.e., tested variance value), the LEO satellite orbits from different prediction time windows, i.e., 0–5 min, 5–10 min, 10–15 min and 15–20 min are used. Without introducing external orbits (S1), the clock precision is about 0.2 to 0.3 ns. Applying S5 and S6, i.e., with relatively weak orbital constraints, leads to improvements for all the tested prediction windows. The S7 shows, in general, the best among these schemes, but it cannot be performed in real-time.

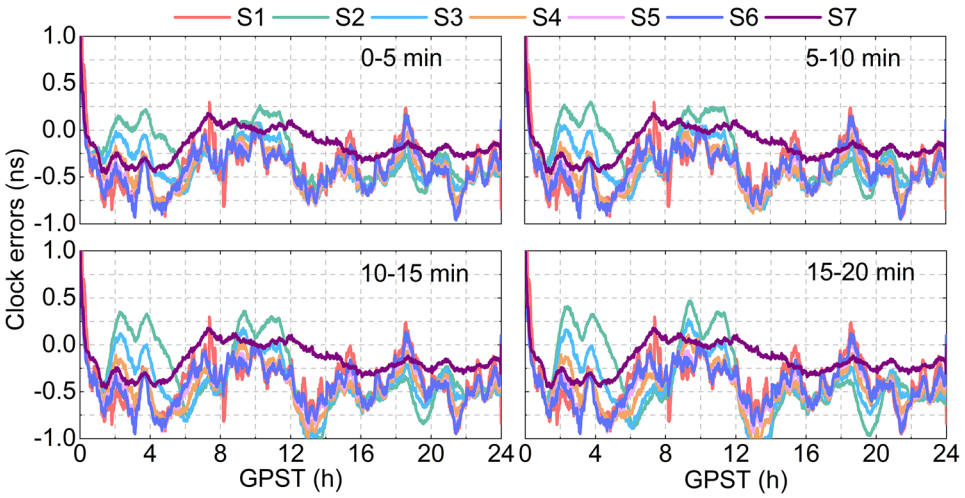

Fig. 6 Clock errors of different schemes on DOY 230, 2018

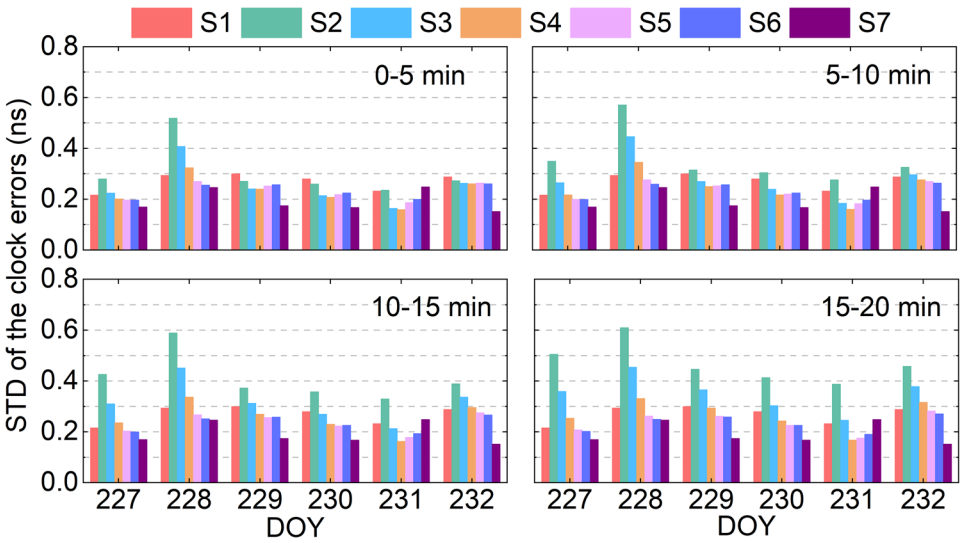

Fig. 7 Daily clock precision applying different schemes introducing orbits of different prediction periods

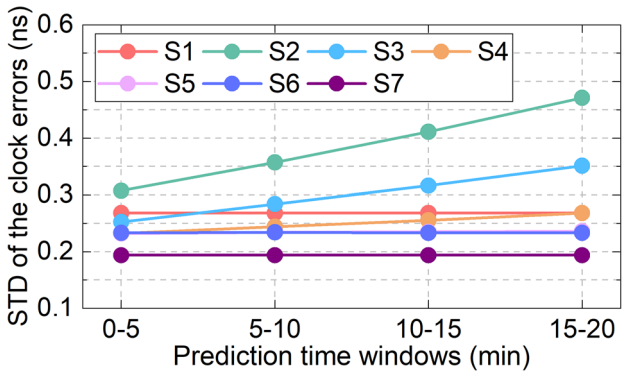

Fig. 8 Average clock precision applying different schemes when constraining orbits of different prediction time windows

The average clock precision applying different schemes is shown in Fig. 8. Although the predicted LEO satellite orbits are not used in S1 and S7, the corresponding results are still shown for the reason of comparison. The average clock precision is 0.268 ns for S1, while for S2 and S3, the clock precision becomes poorer when constraining orbits over prediction periods of 5–10 min or longer. Scheme S2 seems to be a risky option, which leads to a significant increase of the STD to 0.471 ns when constraining orbits from prediction time windows of 15–20 min. After weakening the orbital constraints, i.e., applying S5 and S6, the average clock precision is better than 0.24 ns for all four prediction time windows, with an average STD when applying S5 of 0.232, 0.234, 0.235 and 0.236 ns for prediction periods of 0–5, 5–10, 10–15, 15–20 min, respectively, and 0.233, 0.234, 0.233, and 0.233 ns applying S6, respectively. The clock precision difference introducing orbits of different prediction periods is marginal for S5 and S6. Compared to S1, the improvements in the real-time clock precision for S5 and S6 are about 11.9% to 13.4%. On the other hand, scheme S7 delivers the best solution, with an average clock precision of 0.194 ns.

At the same time, as the estimated LEO clock is constrained by predicted orbits, the actual LEO satellite orbits are simultaneously estimated in real time. Figure 9 shows the real-time LEO satellite orbital errors on DOY 230, 2018, using different schemes when constraining introduced orbits of different prediction periods. The fluctuation of the LEO satellite orbital errors applying S1, i.e., not introducing any orbits, is larger than those of other schemes for all three components, with some spikes visible. At the initialization phase, the orbit convergence is also more obvious when applying S1 than other schemes. When constraining predicted external orbits, the fluctuation in the estimated orbital errors is reduced, with the spikes mentioned before minimized or disappeared. Constraining the orbits strongly to the high-accuracy final orbits (i.e., S7) proves to be very beneficial for orbital estimation but cannot be realized in real time.

Figure 10 shows the estimated daily satellite orbital accuracy in three directions applying different schemes from DOY 227 to 232, 2018. The satellite orbital accuracy of S1 is significantly larger than those of other schemes, while differences in the along-track and cross-track orbital accuracy are small among S2 to S6. It can be observed that the radial orbital accuracy degrades with the weakening orbital constraints. A strong constraint is beneficial for de-correlating the clocks with the radial orbits, thus is favorable for improving the radial orbits. The orbital accuracy of S7 is remarkably better in three directions than applying other schemes.

The average LEO satellite orbital accuracy applying different schemes is shown in Fig. 11. The average satellite orbital accuracy applying Scheme S1 amounts to 6.95, 4.17, and 6.64 cm for the along-track, cross-track, and radial components, respectively. After applying S2 to S7, the orbital

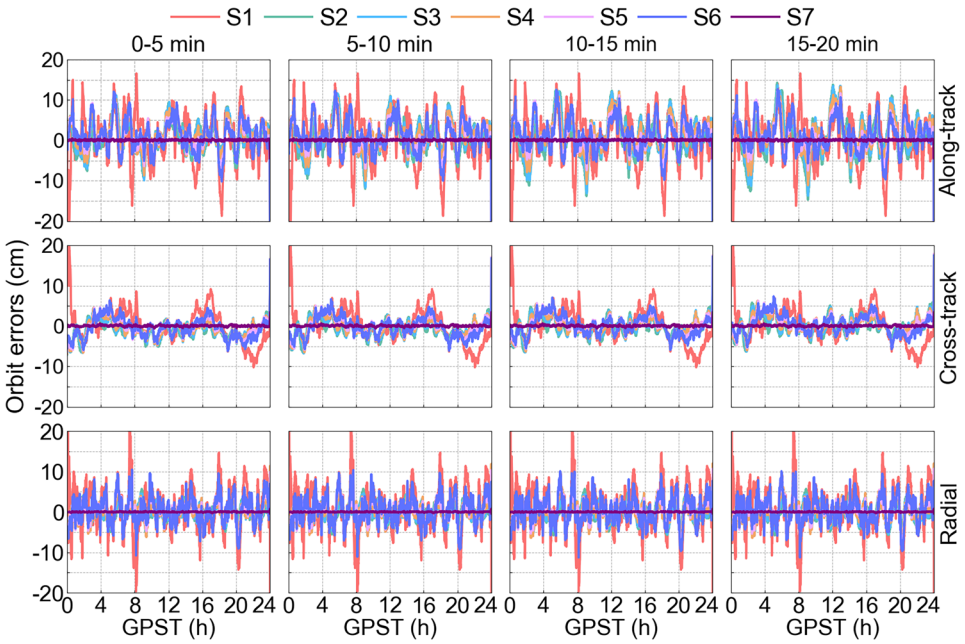

Fig. 9 LEO satellite orbital errors applying different schemes when constraining introduced orbits of different predicted time windows on DOY 230, 2018

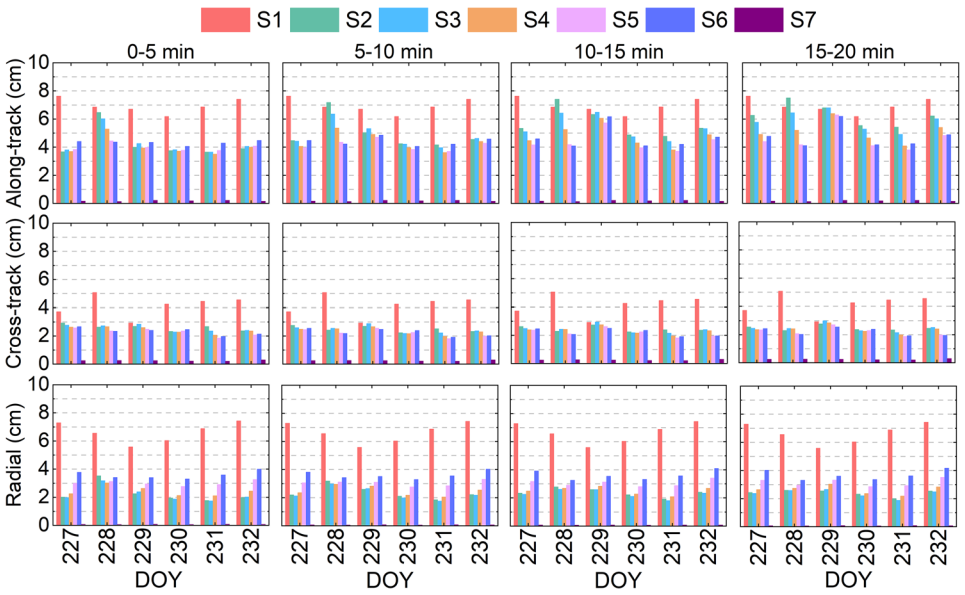

Fig.10 RMSE of the estimated LEO satellite orbits applying different schemes

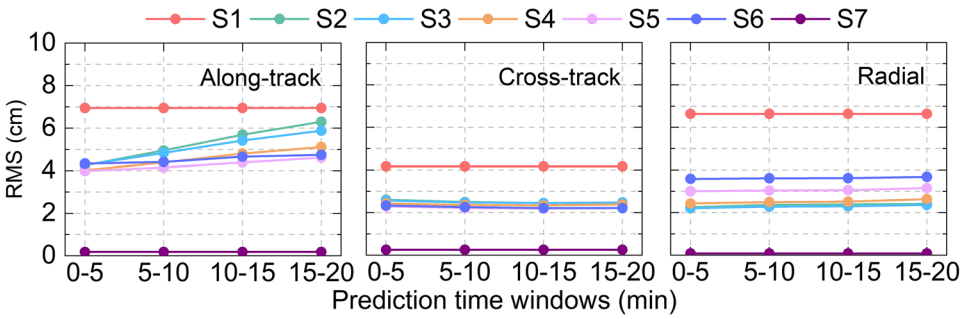

Fig. 11 Average accuracy of the estimated orbits in the along-track (left), cross-track (middle), and radial directions (right) when constraining external orbits of different prediction time windows

accuracy is significantly improved in all three directions. For the along-track component, the S4, S5, and S6 deliver better orbital performances than those of S2 and S3. Because of the degraded introduced orbital accuracy with the increasing predicted period in the along-track direction due to the air drag effects, the accuracy of the estimated orbits is decreased from the prediction period of 0–5 to 15–20 min (see the rising lines in the left panel of Fig. 10). In terms of the cross-track component, the orbital accuracy of each scheme is better than 3 cm, and the differences in the orbital accuracy among different schemes and different prediction periods are marginal. For the estimated radial orbits, the orbit accuracy difference among S2, S3, and S4 is small. On the other hand, the orbit accuracy of S5 and S6 shows poorer performance, which is consistent with Fig. 10. Again, Scheme S7 delivers the best performance in the estimated orbits.

SISRE

SISRE is the projection of the combined LEO satellite orbital and clock errors from the LEO satellite to the Earth in an averaged sense. It can be calculated as:

$$SISRE = \sqrt{(\omega_R \bullet \Delta R - c \bullet dclk)^2 + \omega_{SW}^2(\Delta A^2 + \Delta C^2)} \quad (17)$$

where ΔR, ΔA, ΔC are the estimated satellite orbital errors in the radial, along-track, and cross-track, respectively. ω_R and ω_{sw} are projection coefficients dependent on the orbital heights (Montenbruck et al. 2018), $dclk$ is the clock error, here with the daily mean value removed. Note that the SISRE here refers to an instantaneous value, and differs from the SISRE RMS to be discussed later.

The SISRE time series applying different schemes on DOY 230, 2018, is shown in Fig. 12. Some spikes appeared during 18:00 and 20:00 GPST for S1. After introducing predicted orbits applying S2 to S7, the SISRE of S2 and S3 present larger fluctuations due to the degraded estimated clock precision as shown in Fig. 7. The SISRE of S5 and S6 show almost the same performance, and their fluctuations are less than those of S1, S2, and S3. S7 exhibits the smallest fluctuation of the SISRE series among all tested schemes, which is smaller than 10 cm. Moreover, when using predicted orbits from different prediction time windows to calculate the SISRE, the case using predicted orbits within the 0–5 min of prediction shows the best performance due to the better orbital accuracy achievable within short prediction periods.

Figure 13 presents the SISRE RMS applying different schemes for each day. The SISRE RMS of S1 (red bars) is about 10 cm. After applying S2 and S3, the SISRE RMS is generally increased, and the increase is larger for longer prediction periods due to poorer predicted orbit accuracy. When applying S5 and S6, the SISRE RMS is significantly improved compared to those of S1, while the differences between S5 and S6 are marginal. S7 delivers the best SISRE with the final orbits available and strongly constrained. As the predicted orbital errors are considered biases, not white noise, one often needs to enlarge the variance of the constraint equation but does not use the exact RMS of the introduced predicted orbits. This is also the reason that we tested different variances for the constraint equation when introducing orbits for each prediction window. When the constraints are too strong, e.g., with small variances such as S2 and S3, the orbital biases are pushed to other parameters, e.g., the clocks. Figure 7 suggests that it is safer to use a larger variance when constraining the predicted orbit.

Figure 14 presents the average SISRE RMS applying different schemes constraining orbits of different prediction time windows. The SISRE RMS of S1 is 9.59 cm. For S2 to S6, the average SISRE RMS gradually increases for prediction time windows from 0–5 to 15–20 min, in which the average SISRE RMS of S2 and S3 is 9.6 to 14.89 cm and 8.11 to 11.53 cm, respectively, showing poorer SISRE performances than S1 due to the use of small variances, i.e.,

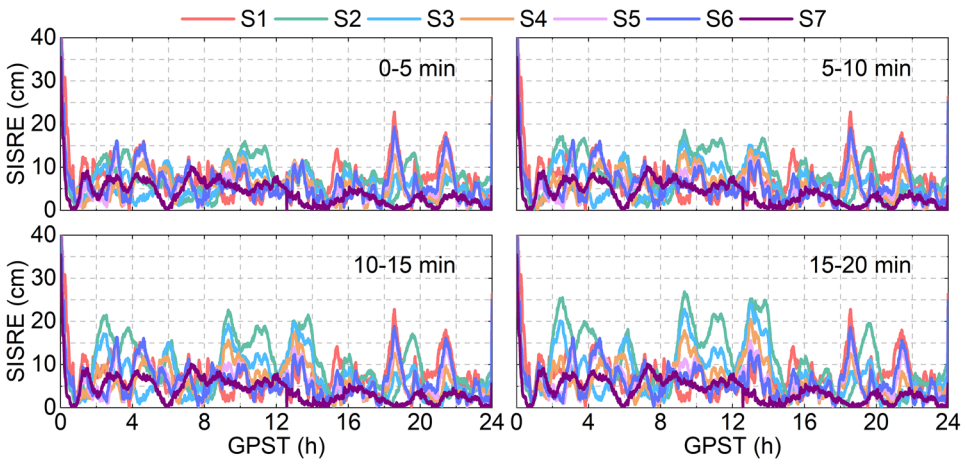

Fig. 12 SISRE time series for Sentinel-3B on DOY 230, 2018, applying different schemes

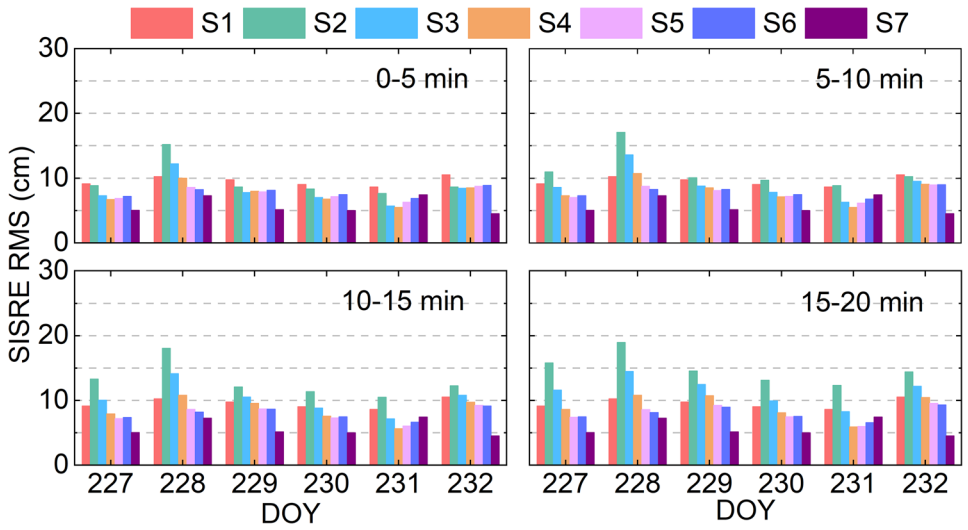

Fig. 13 Daily SISRE RMS for Sentinel-3B applying different schemes

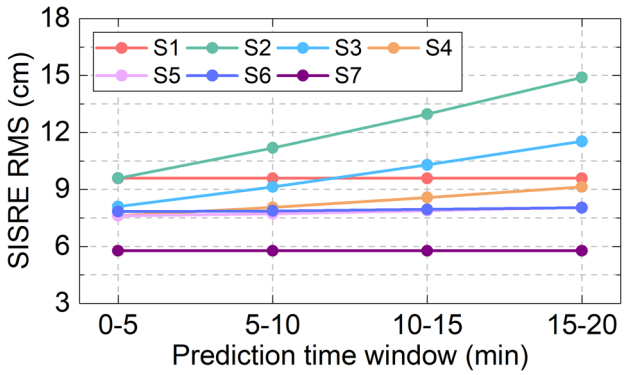

Fig. 14 Average SISRE RMS of Sentinel-3B applying different schemes constraining predicted orbits of different prediction time windows

too strong constraints. Note that the introduced orbital errors are biases but not white noise, variances of the constraint equations need to be larger than the RMS of the introduced orbits. For S4, S5 and S6, the SISRE RMS is smaller than those of S1 for all tested prediction periods, with the performances of S5 and S6 remaining almost the same. The SISRE RMS are 7.62, 7.72, 7.89, and 8.06 cm for S5 at prediction periods of 0–5 min, 5–10 min, 10–15 min and 15–20 min, respectively, and 7.84, 7.87, 7.95, 8.04 cm for S6, respectively. Compared to S1, the SISRE RMS can be improved by 16.0% to 20.5% for S5, and 16.2% to 18.2% for S6. The average SISRE RMS is 5.77 cm for S7, with an improvement of 39.8% compared to that of S1. The SISRE improvements show that the proposed method can effectively improve the real-time LEO satellite clock precision, and eventually the SISRE.

The LEO satellite clock estimation without any orbits constrained is applied in S1, and the SISRE using S5 and S6 shows better performance among these schemes. In real-time mode, ground-based LEO-enhanced PPP needs to be performed using real-time LEO satellite orbits and clocks. When using the KF-based real-time LEO satellite clocks, the real-time LEO satellite orbits from two sources are analyzed and compared for their SISREs. The two compared orbits are the predicted orbits based on the near-real-time BLS POD, and the KF-based real-time kinematic orbits estimated together with the clocks. Therefore, in addition to S1 to S7, another three schemes denoted as $\overline{\text{S1}}$, $\overline{\text{S5}}$, and $\overline{\text{S6}}$, are added to further evaluate the SISRE performance. Instead of the estimated orbital errors, the newly added scenarios use the predicted orbital errors within the different prediction time windows and the estimated clocks to calculate the SISRE. Figure 15 shows the SISRE time series on DOY 230, as a representative example, using S1, $\overline{\text{S1}}$, S5, $\overline{\text{S5}}$, S6 and $\overline{\text{S6}}$ schemes. For S1 (light red of the top panel sub-plots) and $\overline{\text{S1}}$ (deep red of the top panels), the SISRE series introducing predicted orbits shows better performance for most epochs compared to S1. Similarly, for S5, $\overline{\text{S5}}$, S6 and $\overline{\text{S6}}$ schemes, slightly smaller fluctuations are obtained for $\overline{\text{S5}}$ and $\overline{\text{S6}}$ compared to S5 and S6.

The daily SISRE RMS of these six schemes is presented in Fig. 16. It can be observed that the SISRE of $\overline{\text{S1}}$ is better than those of S1 for most days. For DOY 228 and 232, SISRE RMS around or better than 10 cm can be achieved with $\overline{\text{S1}}$, while those of S1 are worse than 10 cm on DOY 228 and 232. For S5 and S6, slight improvements in SISRE can also be obtained for most days when using predicted orbits.

Table 5 presents the average SISRE RMS for these six schemes (S1, $\overline{\text{S1}}$, S5, $\overline{\text{S5}}$, S6 and $\overline{\text{S6}}$). When estimating the clocks without any orbital constraint (S1), the SISRE RMS is 9.59 cm using the estimated orbits. After using the predicted orbits to calculate the SISRE rather than the estimated

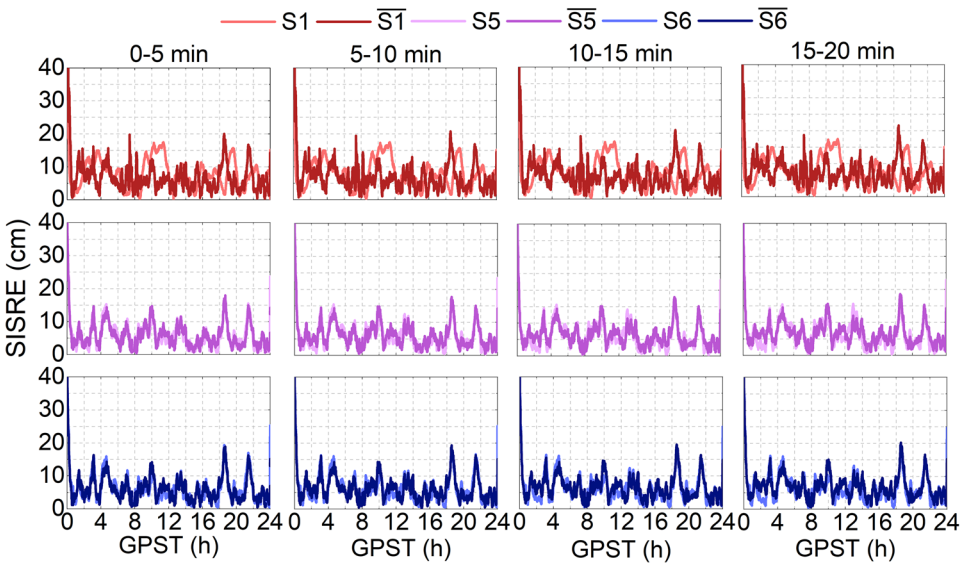

Fig. 15 SISRE time series of Sentinel-3B on DOY 230, 2018, applying Schemes S1, S1, S5, S5, S6 and S6

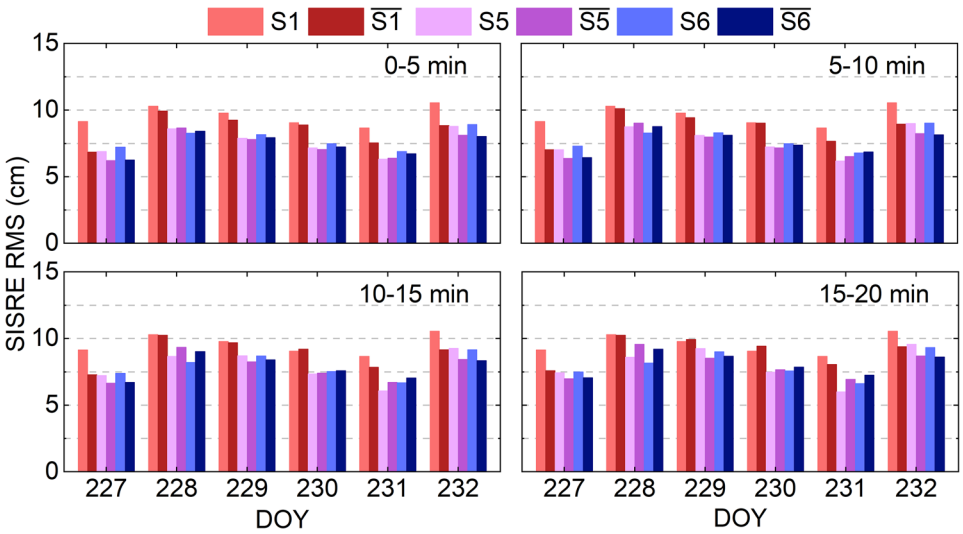

Fig. 16 Daily SISRE RMS of Sentinel-3B applying Schemes S1, S1, S5, S5, S6 and S6

Table 5 Average SISRE RMS applying S1, S1, S5, S5, S6 and S6 schemes

Schemes	0–5 min (cm)	5–10 min (cm)	10–15 min (cm)	15–20 min (cm)
S1	9.59	9.59	9.59	9.59
S1	8.56	8.71	8.91	9.11
S5	7.62	7.72	7.89	8.06
S5	7.38	7.56	7.80	8.07
S6	7.84	7.87	7.95	8.04
S6	7.44	7.63	7.86	8.12

ones, the SISRE RMS can be improved to 8.56, 8.71, 8.91, 9.11 cm for 0–5, 5–10, 10–15, 15–20 min of orbit prediction, with improvements of 10.7%, 9.2%, 7.1% and 5.0%, respectively. For S5, S5, S6 and S6, the SISRE RMS can be slightly improved when calculating SISRE using predicted orbits from prediction periods of 0–5, 5–10, and 10–15 min. However, a slightly worse SISRE can also be found after using predicted orbits from the prediction time window of 15–20 min compared to those using the estimated orbits. In general, after constraining the predicted orbits (within 20 min) during clock estimation, it is still suggested to deliver users with dynamically predicted orbits rather than

the kinematically estimated orbits to achieve a lower SISRE. In general, introducing short-term predicted LEO satellite orbits with proper variances can de-correlate the orbital and clock parameters, strengthen the observation model, and improve both the real-time LEO satellite clock precision and SISRE.

Conclusions

This contribution proposed a method to improve the estimation of real-time LEO satellite clocks by introducing and constraining predicted LEO satellite orbits. Orbits of different prediction time windows are used for the tests applying constraints of different variances.

The proposed method is validated using real GPS data tracked by the LEO satellite Sentinel-3B. The predicted LEO satellite orbits to be introduced in the real-time clock estimation have an RMS of 4.57, 5.31, 6.00, and 6.63 cm for prediction periods 0–5 min, 5–10 min, 10–15 min, and 15–20 min, respectively, for the along-track components. The predicted cross-track and radial orbits are generally better. Seven schemes (S1 to S7) were investigated to test the impact of different variances when constraining the introduced orbits. Without introducing any orbits, the real-time clock estimates exhibit a precision of 0.268 ns. After weakly constraining the orbits with a standard deviation of 4–6 dm in the along-track direction, and 2–3 dm in the other two directions (Schemes S5 and S6), the clock precision can be improved to 0.232, 0.234, 0.235, and 0.236 ns applying S5 when constraining orbits at prediction periods 0–5 min, 5–10 min, 10–15 min, 15–20 min, respectively. The clock precision improved to 0.233, 0.234, 0.233, and 0.233 ns applying S6, respectively. Compared to the case of not introducing orbits, the improvements of the clock precision applying S5 and S6 amount to about 11.9 to 13.4%, respectively. When strongly constraining the orbits to the reference orbits, the clock precision can be improved to below 0.2 ns.

As of the SISRE RMS, it was found that in case of not introducing any orbits, it is preferable to provide the short-term predicted orbits to real-time navigation users instead of the kinematic orbits estimated together with the clocks. The SISRE RMS in the former case is from 8.56 to 9.11 cm for different prediction time windows from 0–5 min to 15–20 min, while it amounts to 9.59 cm for the latter case. Using the estimated clocks and orbits after constraining the external predicted orbits, the SISRE RMS are reduced to 7.62, 7.72, 7.89, and 8.06 cm when weakly constraining the orbits with a standard deviation of 4 dm, 2 dm and 2 dm in the along-track, cross-track and radial directions (S5) at prediction periods of 0–5 min, 5–10 min, 10–15 min and 15–20 min, respectively. It can be reduced to a similar level of 7.84, 7.87, 7.95, 8.04 cm when applying even weaker constraints on orbits of the four prediction periods with a standard deviation of 6 dm, 3 dm, and 3 dm in these three directions (i.e., S6). Compared to the case of not introducing any orbits (S1), the SISRE RMS can be improved from 16.0 to 20.5% by applying S5, constraining orbits of the four prediction periods, and 16.2 to 18.2% for S6. The average SISRE RMS is 5.77 cm when strongly constraining to the reference orbits, with an improvement of 39.8% compared to S1. Using the estimated clocks and predicted orbits in $\overline{S5}$ and $\overline{S6}$, it was found that the SISRE RMS from prediction time windows of 0–5, 5–10, and 10–15 min is slightly better than those of using estimated orbits and clocks. Applying $\overline{S5}$ using predicted orbits from a prediction time window of 0–5 min, the SISRE RMS is improved to 7.38 cm, with an improvement of 23.0% compared to S1.

Acknowledgements We would like to acknowledge the support of the international GNSS monitoring and assessment system (iGMAS) at the National Time Service Center, and the National Space Science Data Center, National Science & Technology Infrastructure of China (http://www.nssdc.ac.cn).

Authors' contributions KW provided the initial idea and designed the experiments for this study; WX and MZ analyzed the data and wrote the manuscript; and KW, HS, JL, MW, MZ, AE and XY helped with the writing. All authors reviewed the manuscript.

Funding This work is supported by the International Partnership Program of the Chinese Academy of Sciences. Grant No. 021GJHZ2023010FN. The work is also funded by the National Time Service Center, Chinese Academy of Sciences (CAS) (No. E167SC14), the National Natural Science Foundation of China (No. 12073034, 12203059), the special research assistant funding project, CAS (110400T0XW), and the Australian Research Council—Discovery Project No. DP240101710.

Data availability The GNSS observations from Sentinel-3B are available at https://scihub.copernicus.eu/gnss/#/home. The CNES real-time GNSS products are available at http://www.ppp-wizard.net/products/REAL_TIME/.

Declarations

Conflict of interest The authors declare no competing interests.

Ethical approval This manuscript does not report on or involve the use of any animal or human data or tissue.

Consent for publication All authors approved the final manuscript and the submission to this journal.

References

Beutler G (2005) Variational equations. In: Methods of celestial mechanics; astronomy and astrophysics library. Springer, Berlin, pp 175–207

Duan B, Hugentobler U, Chen J, Selmke I, Wang J (2019) Prediction versus real-time orbit determination for GNSS satellites. GPS Solut 23(2):39

El-Mowafy A, Wang K, Li Y, Allahvirdi-Zadeh A (2023) The impact of orbital and clock errors on positioning from LEO constellations and proposed orbital solutions. Arch Photogramm Remote Sens Spatial Inf Sci, XLVIII-1/W2-2023, pp 1111–1117

Fu W, Chen R, Cui Y (2023) A computationally efficient prior quality control approach for multi-GNSS real-time satellite clock estimation. GPS Solut 27(4):177

Ge H, Wu T, Li B (2023) Characteristics analysis and prediction of Low Earth Orbit (LEO) satellite clock corrections by using least-squares harmonic estimation. GPS Solut 27(1):38

Huang G, Cui B, Zhang Q, Fu W, Li P (2018) An improved predicted model for BDS ultra-rapid satellite clock offsets. Remote Sens 10:60

Kalman RE (1960) A new approach to linear filtering and prediction problems. J Basic Eng 82(1):35–45

Ke M, Lv J, Chang J, Dai W, Tong K, Zhu M (2015) Integrating GPS and LEO to accelerate convergence time of precise point positioning. In: Proceeding of the 7th international conference on wireless communications and signal, IEEE, pp 1–5

Kouba J (2009) A guide to using international GNSS service (IGS) products. ftp://igs.org/pub/resource/pubs/UsingIGSProductsVer21_cor.pdf.

Kunzi F, Montenbruck O (2022) Precise onboard time synchronization for LEO satellites. Navigation 69(3):531

Laurichesse D, Cerri L, Berthias JP, Mercier F (2013) Real time precise GPS constellation and clocks estimation by means of a Kalman filter. In: Proceedings of the ION GNSS+, Institute of Navigation, Nashville, TN, USA, 16–20 Sept 2013; pp 1155–1163

Li K, Zhou X, Guo N, Zhao G, Xu K, Lei W (2017) Comparison of precise orbit determination methods of zero-difference kinematic, dynamic and reduced-dynamic of GRACE-A satellite using SHORDE software. J Appl Geodesy 11(3):157–165

Li X, Li X, Ma F, Yuan Y, Zhang K, Zhou F, Zhang X (2019a) Improved PPP ambiguity resolution with the assistance of multiple LEO constellations and signals. Remote Sens 11:408

Li X, Ma F, Li X, Lv H, Bian L, Jiang Z, Zhang X (2019b) LEO constellation-augmented multi-GNSS for rapid PPP convergence. J Geod 93(5):749–764

Li X, Qin Y, Zhang K, Wu J, Zhang W, Zhang Q, Zhang H (2022) Precise orbit determination for LEO satellites: single-receiver ambiguity resolution using GREAT products. Geo-Spat Inf Sci 25(1):63–73

Li W, Yang Q, Du X, Li M, Zhao Q, Yang L, Qin Y, Chang C, Wang Y, Qin G (2024) LEO augmented precise point positioning using real observations from two CENTISPACE™ experimental satellites. GPS Solut 28(1):44

Lyard F, Lefevre F, Letellier T, Francis O (2006) Modelling the global ocean tides: modern insights from FES2004. Ocean Dyn 56:394–415

Mao X, Arnold D, Girardin V, Villiger A, Jäggi A (2021) Dynamic GPS-based LEO orbit determination with 1 cm precision using the Bernese GNSS software. Adv Space Res 67(5):788–805

Montenbruck O, Steigenberger P, Hauschild A (2018) Multi-GNSS signal-in-space range error assessment–methodology and results. Adv Space Res 61(12):3020–3038

Pavlis NK, Holmes SA, Kenyon SC, Factor JK (2008) An earth gravitational model to degree 2160: EGM2008. In: Proceedings of the EGU 2008, Vienna, Austria, 13–18 Apr 2008

Petit G, Luzum B (2010) IERS conventions; IERS Technical Note, 36; Verlag des Bundesamts für Kartographie und Geodäsie: Frankfurtam Main, Germany, 2010, ISBN 3-89888-989-6

Prange L, Orliac E, Dach R, Arnold D, Beutler G, Schaer S, Jäggi A (2017) CODE's five-system orbit and clock solution-the challenges of multi-GNSS data analysis. J Geod 91(4):345–360

Standish EM (1998) JPL Planetary and Lunar Ephemerides, DE405/LE405. JPL IOM 312, F-98–048

Wang K, El-Mowafy A (2022) LEO satellite clock analysis and prediction for positioning applications. Geo-Spat Inf Sci 25(1):14–33

Wang K, El-Mowafy A, Yang X (2022a) URE and URA for predicted LEO satellite orbits at different altitudes. Adv Space Res 70(8):2412–2423

Wang K, Yang X, El-Mowafy A (2022b) Visibility of LEO satellites under different ground network distributions. In Proc ION GNSS+ 2022, Denver, Colorado, USA, Sept 2022, pp 2478–2491

Wang K, El-Mowafy A, Su H, Yang X (2023a) On the very short and very long LEO satellite orbit prediction. In Proc ION ITM 2023, Long Beach, CA, USA, Jan 23–26, 2023, pp 725–735

Wang K, Liu J, Su H, El-Mowafy A, Yang X (2023b) Real-time LEO satellite orbits based on batch least-squares orbit determination with short-term orbit prediction. Remote Sens 15:133

Wu M, Wang K, Liu J, Zhu Y (2023) Relativistic effects of LEO satellite and its impact on clock prediction. Meas Sci Technol 34:095005

Xie W, Huang G, Wang L, Li P, Cui B, Wang H, Cao Y (2021) Long-term performance detection and evaluation of GLONASS onboard satellite clocks. Measurement 175:109091

Yang Z, Liu H, Qian C, Shu B, Zhang L, Xu X, Zhang Y, Lou Y (2020) Real-time estimation of low Earth orbit (LEO) satellite clock based on ground tracking stations. Remote Sens 12(12):205

Yang Z, Liu H, Wang P, Xu X, Qian C, Shu B, Zhang Y (2022) Integrated kinematic precise orbit determination and clock estimation for low Earth orbit satellites with onboard and regional ground observations. Meas Sci Technol 33(12):125002

Yunck TP, Bertiger WI, Wu SC, Bar-Sever YE, Christensen EJ, Haines BJ, Lichten SM, Muellerschoen RJ, Vigue Y, Willis P (1994) First assessment of GPS-based reduced dynamic orbit determination on TOPEX/Poseidon. Geophys Res Lett 21(7):541–544

Zhou F, Wang X (2023) Some key issues on pseudorange-based point positioning with GPS, BDS-3, and galileo observations. Remote Sens 15(3):797

Wei Xie is currently an assistant researcher at National Time Service Center, Chinese Academy of Science. He received his phD from Chang'an University, Xi'an, P.R. China in July, 2023. His research area is LEO satellite clock estimation, GNSS realtime satellite clock estimation and satellite clock performance evaluation.

Hang Su is an associate professor at the National Time Service Center, Chinese Academy of Sciences. She received her Ph.D. in astrometry and celestial mechanics from the University of Chinese Academy of Sciences in 2022. Her research interests include tropospheric delay in GNSS, LEO satellite POD and clock determination.

Kan Wang is a Professor at the National Time Service Center, Chinese Academy of Sciences. She received her PhD in GNSS advanced modelling from ETH Zurich in 2016 and worked at Curtin University until 2021. Her research interests include high-precision GNSS positioning, LEO-related topics and integrity monitoring.

Jiawei Liu is an Assistant Professor at the College of Mechatronics and Control Engineering, Shenzhen University. He has received his Ph.D. degree at South China University of Technology of China in 2015. He His research interests include dry electrical discharge dressing and truing of diamond grinding wheel, precision grinding of hard and brittle semiconductor materials, dry electrical discharge grinding process of metal matrix composites, and microstructure manufacturing technology for microfluidic chip and LED light guide.

Meifang Wu is a senior engineer in the National Times Service Center (NTSC). She received her Ph.D. degree in astrometry and celestial mechanics from the University of Chinese Academy of Sciences (CAS), China, in 2017. Her research currently focuses on GNSS real-time clock determination and real-time time service technologies.

Min Zou is currently a master's student at the National Time Service Center, Chinese Academy of Sciences. He received his bachelor's degree from Harbin Normal University in 2020. His research focuses on precise orbit determination of LEO satellites.

Ahmed El-Mowafy is a Professor and Director of Graduate Research, School of Earth and Planetary Sciences, Curtin University, Australia. He obtained his PhD from the University of Calgary, Canada, in 1995, and has more than 200 publications in precise positioning and navigation using GNSS, quality control, POD, integrity monitoring and estimation theory.

Xuhai Yang is currently a National Time Service Center researcher, Chinese Academy of Sciences, Xi'an, China. He received his Ph.D. degree in astrometry and celestial mechanics from the Graduate School of the Chinese Academy of Sciences, Beijing, China, in 2003. His scientific interests include highprecision time transfer, orbit measurements, and orbit determination.